Highlights

Electric Vehicle Range Extension Using Nonlinear MPC Based Active Battery Cell Balancing

Afaq Ahmed, Ali Arshad Uppal, Qadeer Ahmed

- High-fidelity mathematical modeling of generalized N-serially connected cells.
- Formulation and subsequent solution for the NMPC problem to perform cell balancing; moreover, stability guarantees are provided.
- Demonstration of range extension as a result of ACB under NMPC for diversified real-world scenarios.
- Statistical analysis and quantification of the impact of certain parameters on EV's range.

Electric Vehicle Range Extension Using Nonlinear MPC Based Active Battery Cell Balancing

Afaq Ahmed[a], Ali Arshad Uppal[a], Qadeer Ahmed[b]

[a]*Department of Electrical Engineering, COMSATS University Islamabad, Islamabad, 45550, Pakistan*
[b]*Mechanical and Aerospace Engineering, The Ohio State University, Columbus, 43210-1142, OH, USA*

Abstract

Cell balancing is one of the crucial tasks of the battery management system (BMS) within an electric vehicle (EV) to enhance the battery's performance. This research focuses on developing a non-linear model predictive control (NMPC) to actively balance multiple cells connected in series in the battery pack of an EV. The goal is to improve EV range by formulating NMPC problem employing high-fidelity models of balancing currents and power losses for buck-boost converter based active cell balancing network. Moreover, the stability of the generalized N serially connected cells is demonstrated by utilizing Lyapunov theory. Similarly, various cost functions are incorporated into the NMPC framework, and a thorough statistical analysis, using a comprehensive dataset, is conducted. The impact of driving conditions, NMPC's cost functions and initial state of charge (SoC) levels on the EV's range, balancing time, and power losses is evaluated. Upon balancing under NMPC framework, the comparision with no-balancing scenario demonstrates a maximum range increase of 39.2 km, and a minimum increase of 17.4 km in certain drive cycles; whereas an average increase of 28.9 km is achieved for all drive

cycles.

Keywords: Electric vehicles, Lithium-ion batteries, range extension, active cell balancing, nonlinear model predictive control

1. Introduction

Electric vehicles (EVs) can play a prominent role in addressing concerns related to energy and pollution by reducing fuel expenses and eliminating harmful emissions [1]. In this regard, a battery management system (BMS) is incorporated to ensure that EV's battery gives optimal performance by keeping homogeneous operating conditions across the battery pack. Among others, BMS primary functionalities include monitoring and regulating critical battery parameters such as voltage, current, temperature, and state of charge (SoC), etc.

One of the immediate concerns, especially from the end user's perspective, related to EVs is the issue of range anxiety. There are multiple reasons underlying this; however, charge imbalance among cells is a foremost factor that is addressable by BMS. The issue of cell-to-cell imbalance arises in series connected cells where the full depletion of any single cell's charge causes the string to shut down. If not addressed, the issue of cell imbalance can lead to persistent degradation of the battery pack. To overcome this, cell balancing can play a crucial role. This can be achieved by two main approaches: passive and active cell balancing (ACB) [2]. ACB is preferred over the passive approach, as it reduces the energy losses by including power electronic devices, which act as intermediate energy storage components.

Evidently, ACB is usually achieved within a closed-loop framework, em-

ploying techniques from both classical and contemporary classes. In this regard, model predictive control (MPC) has emerged as a viable technique in the ACB paradigm. This is primarily due to the fact that MPC can handle multiple conflicting objectives, tackle nonlinear and coupled systems, and respect constraints on plant inputs and outputs [3]. However, these diverse functionalities imply that there are multiple design parameters-appropriate choice of cost function, fine-tuning parameters, stability, robustness, etc.– that need to be carefully taken care of, as these undergird the desired closed-loop performance, i.e., range extension. The next section will discuss the applications of ACB as undertaken in the state of the art, particularly in the context of EV's range and other performance metrics.

1.1. Literature Review

Inherent heterogeneity is one of the primary factors driving the need for cell balancing [4]. In this respect, [5] quantified the impact of cell imbalance on EV range. By simulating the 125 drive trips, the authors identified that cell capacity is the most significant factor affecting the EV's range. On the same topic, [6] investigated even more factors that influence EV's range by categorizing them into 4 major groups: vehicle design, BMS, driver, and environment. Moreover, the authors noted that most of the factors related to the vehicle and driver are encoded by drive cycles. In effect, there have been multiple studies employing cell balancing to bypass these drawbacks. For instance, [7] used the nonlinear MPC (NMPC) framework to perform ACB by simultaneously minimizing the SoC difference and energy dissipation in the balancing network. Though the simulations were performed on two cells only, the authors also took into consideration the computational burden of

the control scheme to facilitate the implementation of real-time control. In the same context of addressing the MPC computational burden, [8] proposed to integrate reinforcement learning (RL) with MPC. With RL acting as an optimal policy to trigger the MPC to solve the optimization problem, the work demonstrated that triggering occurred on average in 1000 s as compared to 1 s of baseline MPC. While reducing the computational burden, the framework simultaneously achieved a maximum range of up to 48 km. Similarly, other studies have quantified the efficacy of ACB in range extension; [9] proposed to set a theoretical benchmark for maximal range achievable as a result of ACB under ideal conditions. They posed this problem as reachability analysis, and by running the simulation on 10 cells, the authors reported an increase of 23 s in battery runtime compared to no balancing. In the same context of MPC-based ACB for range extension, [10] explored various objectives that comprised voltage, SoC, and charge-based quantities. In the same vein, using the feasibility approach, [11] demonstrated a 5% extension in the range and a 10% prolongation in end-of-life (EoL). Moreover, different variants of MPC formulation in terms of objective functions have been investigated by [12]. Overall, 7% and 4% range enhancements were reported in steady-state and transient scenarios, respectively. Consequently, in [13], the authors also considered unfamiliar driving patterns and showcased the robustness of MPC based balancing in the face of these uncertainties. Beyond the application of MPC during discharging to exhibit range extension, it has also been utilized for balancing during charging. For instance, [14] formulated a multi-objective optimal control problem to charge the battery quickly while keeping its degradation to a minimum. Similar kind of work has also been taken up by [15] in

the NMPC framework; though the proposed strategy took longer to charge than traditional voltage-based approaches, it met the desired performance parameters while meeting the safety and computational constraints. The authors in [16] designed balancing aware NMPC for capacitor, and inductor based ACB networks (ACBNs), and compared their performance during overnight charging. The analysis demonstrated that capacitor based ACBN yielded superior performance compared to its counterpart. Moreover, there have been additional studies incorporating various balancing topologies and control algorithms aimed at achieving diversified objectives: from cell balancing to temperature regulation, reduced charging times, and range extension cf. [17, 18, 19]. Additionally, the researchers have also utilized statistical tools to quantify the impact of variations in battery parameters, such as capacity and charging profiles, on underlying performance [20].

1.2. Gap Analysis

In the literature, multiple control strategies have been implemented for ACB, and similarly, there has also been statistical analysis on quantifying the impact of various factors on ACB performance. However, there are some avenues that are not thoroughly investigated. For instance, (i) in considering the control formulation of the ACBN, especially under MPC's framework, the problem is usually posed for a finite number of serially connected cells, with the fidelity of the underlying ACBN model kept to a minimum. (ii) By the same extension, the stability analysis of the closed-loop systems is performed for the same limited problem formulation. Moreover, as highlighted in the literature review, the range of an EV is influenced by a number of factors pertaining to battery, vehicle, and control techniques. However, (iii) there

exist limited studies that systematically quantify the impact of variables such as drive cycle, cost function, initial SoC configuration, etc., on ACBN performance metrics.

In our earlier works, we proposed high-fidelity mean current and power losses models for capacitor, inductor, and transformer-based ACBN for two series connected cells [21, 22]. Therein, we demonstrated that considering the dynamic and static parameters of ACBN is crucial in accurately determining the ACBN performance. Building upon the mean balancing current approach, we devised a power loss-aware NMPC formulation for inductor-based ACBN in [23]. Despite increasing the fidelity, the two-cell-based model is insufficient to capture the impact of ACBN on EV's range. This is because in series-based adjacent cell-cell configuration, the total number of ways in which charge can be transferred among cells can't be modeled by two cells. Therefore, keeping in mind the need for a generalized ACBN model comprising N cells for control problem formulation and the subsequent quantification of important parameters on EV's range, the major contributions of this work are iterated as follows:

1.3. Major Contributions

1. Mathematical modeling of high-fidelity mean balancing currents and power losses of a generalized N-cells ACBN based on buck-boost converter (BBC) for series-based cell-cell topology.
2. Formulation of a generalized NMPC problem with three distinct balancing-aware cost functions; the problem is subsequently solved, and stability guarantees are provided.

3. System-level manifestation of ACB in terms of range extension by solving the ACB control problem. Moreover, extensive simulations are conducted to demonstrate robustness in the face of various drive cycles. Furthermore, a multivariate analysis of variance (MANOVA) is carried out to study the impact of different cost functions, varying driving conditions, and the cells' SoC configuration on the EVs range, balancing time, and power losses.

The subsequent sections of the paper unfold as follows: section 2 develops the higher-dimensional mathematical modeling of the ACBN; section 3 formulates and solves the NMPC problem for the ACBN and establishes proof of the stability and convergence of the same. A detailed discussion on ACBN's results and the consequent statistical analysis is given in section 4; and finally, the paper reaches its conclusion in section 5.

Table 1: List of symbols

Symbol	Description
N, x_n	Number of serially connected cells in a battery pack and Cell's SoC [%]
u_{ij}, SoC	Duty cycles of MOSFETS and state of charge (%) of cell, respectively
I_{b_n}, I_e	Current of cell n, and Load current, respectively (A)
η_n, R_{0_n}	Cell's capacity (As) and internal resistance of cell n (Ω), respectively
L_i, $D_{i,j}$,$Q_{i,j}$	Inductor, Diode, and MOSFETS, respectively
I_{ch}, I_{dis}	Effective current during charging and discharging modes of buck-boost (A)
$V_{F_{i,j}}$, v_{ti}	Forward voltage drop of diode $D_{i,j}$ and cells' terminal voltage (V)
τ_c, τ_d	Time constants for charging and discharging of L_i, respectively (s)
t_d, t_{0_i}, T	Dead time, time instant at which L_i current is 0, and switching time period, respectively (s)
R_{L_i}, R_{ds}, R_{c_i}, R_{d_i}	Resistances of L_i, on-state switching and charging and discharging paths of L_i, respectively (Ω).
P_{con}, P_{t_f}	Overall conduction power losses and switching losses when Q_{ij} is on, respectively (W)
$P_{D_{rr}}$,P_{t_d}	Reverse recovery power loss associated with D_{ij}, and dead time power losses, respectively (W)
$\mathcal{I}_{c_{i,j}}$, $\mathcal{I}_{d_{i,j}}$	Charging and discharging RMS currents (A)
$v_n, \sigma(.)$	Open circuit voltage of a cell (V) and standard deviation of SoC levels.
$t_b, \bar{P}_T$	Balancing time and average power losses (total) during balancing.
t_c, t_{sim}	Computational and simulation times.
ACB, ACBN	Active cell balancing and active cell balancing network.
Li-ion, ECM	Lithium ion and equivalent circuit model.
	Buck-boost based converter and model predictive control
ANOVA, MAVOVA	Analysis of variance and multivariate analysis of variance.

2. Mathematical Modelling of ACBN

The ACBN–as represented in Figure 1– comprises two parts: (i) a battery pack containing N serially connected cells and (ii) a balancing network containing $(N-1)$ BBCs with $2\times(N-1)$ MOSFETs. Although a simple equivalent circuit model (ECM) is used to represent the dynamics of Li-ion cells, high-fidelity mathematical models of mean balancing current and power losses of balancing network are considered. These high-fidelity models are adopted from [22] and extended to an N-cell configuration in this work.

2.1. Equivalent Circuit Model of the Cell

The equations representing SoC levels and terminal voltages of cells are given as

$$\dot{\mathbf{x}} = \mathbf{f}(\mathbf{x},\mathbf{u}), \tag{1}$$

$$\mathbf{v}_t = \mathbf{h}(\mathbf{x},\mathbf{u}), \tag{2}$$

$$\mathbf{f}(\mathbf{x},\mathbf{u}) = \begin{bmatrix} \dfrac{I_{b_1}(\mathbf{x},\mathbf{u})}{\eta_1} & \dfrac{I_{b_2}(\mathbf{x},\mathbf{u})}{\eta_2} & \cdots & \dfrac{I_{b_N}(\mathbf{x},\mathbf{u})}{\eta_N} \end{bmatrix}^T,$$

$$\mathbf{h}(\mathbf{x},\mathbf{u}) = \begin{bmatrix} v_1(x_1) + I_{b_1}(\mathbf{x},\mathbf{u})R_{0_1} \\ v_2(x_2) + I_{b_2}(\mathbf{x},\mathbf{u})R_{0_2} \\ \vdots \\ v_N(x_N) + I_{b_N}(\mathbf{x},\mathbf{u})R_{0_N} \end{bmatrix},$$

$$v_n = \sum_{s=1}^{8} p_s x_n^{(8-s)}, \tag{3}$$

where the state vector $\mathbf{x} = \begin{bmatrix} x_1 & x_2 & \dots & x_N \end{bmatrix}^T$ represents the SoC levels of N cells; $\mathbf{v}_t = \begin{bmatrix} v_{t_1} & v_{t_2} & \dots & v_{t_N} \end{bmatrix}$ is the vector of cells' terminal voltages (V); $\mathbf{f} : \Re^N \times \Re^{2(N-1)} \to \Re^N$ and $\mathbf{h} : \Re^N \times \Re^{2(N-1)} \to \Re^N$ are smooth nonlinear

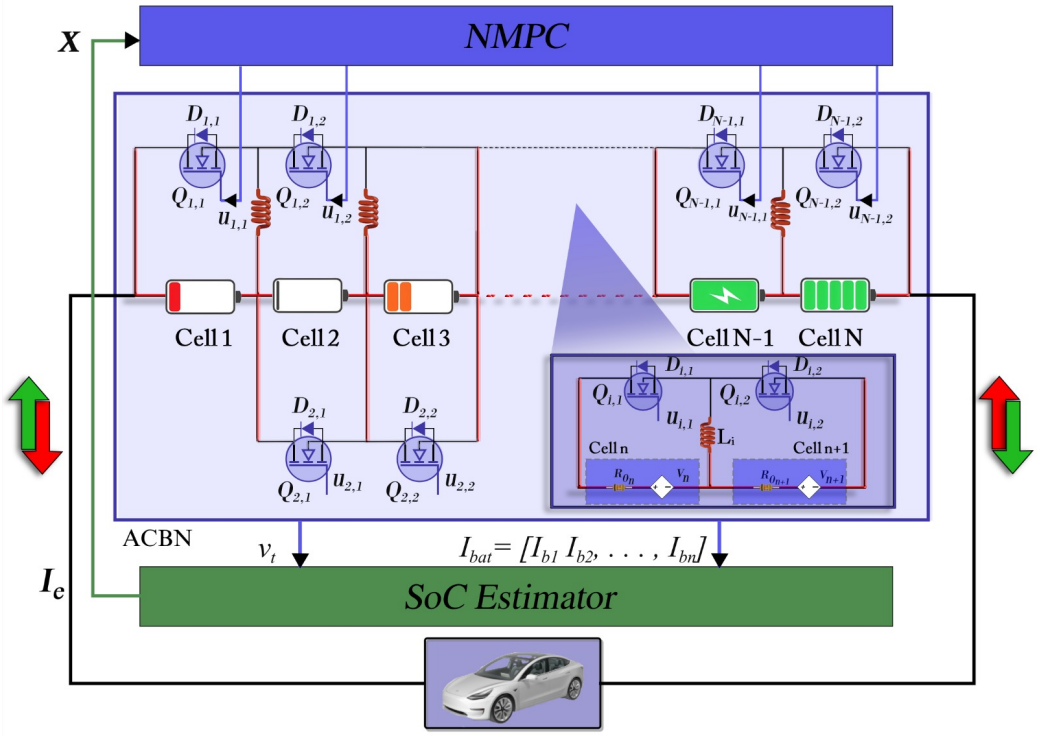

Figure 1: Closed-loop system showing the Interaction of an ACBN, NMPC and SoC estimator. Moreover, the drive cycle current I_e is also shown.

functions of $\mathbf{x}$, and $\mathbf{u}$, where $\mathbf{u} = \{u_{i,j}\}$ is the control input vector, representing the duty cycles of MOSFETS; η_n represents the cell capacity in (As), and I_{b_n} is the effective current (A) of cell n, and $n = 1, 2, \cdots, N$; the internal resistance of cell n is denoted by R_{0_n} (Ω); and v_n represents the open circuit voltage (OCV) of a cell, and $p = [88.56, -320.46, 472.36, -368.96, 166.57, -44.01, 7.18, 2.95]$ is the polynomial representing the relationship between cell's SoC and OCV. Depending on the positioning of a cell in the battery pack, the expressions for cells' currents are given as

$$
\begin{aligned}
I_{b_1} &= -I_e - I_{c_{1,1}}(x_1, u_{1,1}) + I_{d_{1,2}}(x_1, x_2, u_{1,2}) - I_{Loss}, \\
I_{b_{n\neq 1,N}} &= -I_e - I_{c_{n,1}}(x_n, u_{n,1}) + I_{d_{(n-1),1}}(x_{n-1}, x_n, u_{(n-1),1} \\
&\quad - I_{c_{(n-1),2}}(x_n, u_{(n-1),2}) + I_{d_{n,2}}(x_n, x_{n+1}, u_{n,2}) - I_{Loss}, \\
I_{b_N} &= -I_e - I_{c_{(N-1),2}}(x_N, u_{(N-1),2}) - I_{Loss} \\
&\quad + I_{d_{(N-1),1}}(x_{N-1}, x_N, u_{(N-1),1}),
\end{aligned} \tag{4}
$$

where $I_{c_{i,j}}$ and $I_{d_{i,j}}$ are charging and discharging currents (also known as balancing currents) of inductor i when MOSFET $Q_{i,j}$ is turned on, respectively, and $i = 1, 2, \cdots, (N-1)$ and $j = 1, 2$ represent the number of BBCs and MOSFETs per converter, respectively; I_e is the external load current as shown in Figure 1; $I_{Loss} = P_T / \left(\sum_{n=1}^{N} v_{t_n}\right)$ represents the loss current that accounts for the power losses; and P_T is the total power loss, cf. (11).

In this work, charge transfer is accomplished by employing series-based cell-to-cell topology [24]. As shown in Figure 1, there is a dedicated BBC to balance the charge between two adjacent cells. The mean balancing currents responsible for equalizing the SoC levels of cells n and $n+1$ (zoomed portion

in Figure 1) are $I_{c_{i,1}}$, $I_{d_{i,1}}$, $I_{c_{i,2}}$ and $I_{d_{i,2}}$. When $x_n > x_{n+1}$, the MOSFET $Q_{i,1}$ is turned on employing $u_{i,1}$ and the current $I_{c_{i,1}}$ starts charging the inductor L_i. The stored charge in L_i is transferred to x_{n+1} when $I_{d_{i,1}}$ flows through the diode $D_{i,2}$ when both $Q_{i,1}$ and $Q_{i,2}$ are off. Similarly, $I_{c_{i,2}}$ and $I_{d_{i,2}}$ transfer the excess charge from x_{n+1} to x_n when $x_{n+1} > x_n$ by utilizing $u_{i,2}$. To avoid short circuit both MOSFETs $Q_{i,1}$ and $Q_{i,2}$ can not be turned on simultaneously. In series-based cell-cell topology, a cell sandwiched between two cells receive/transfer current from/to two adjacent BBCs while the first and the last cells are linked with only one BBC, cf. (4). The balancing currents given in (5) and (6) are positive; however, the negative sign with charging current in (4) is due to the current convention considered in this article–any current exiting a cell is negative, whereas a positive sign is used with the currents entering a cell.

2.2. Mean Balancing Currents

The high-fidelity models of the balancing currents $I_{c_{i,j}}$ and $I_{d_{i,j}}$, which take into account the effect of various static and dynamic ACBN parameters are adapted from [22], and are generalized in the following manner

$$I_{c_{i,j}} = \frac{v_h}{TR_{c_i}}\bigg(u_{i,j}T - t_d + \tau_{c_i}\left(e^{\kappa_i} - 1\right)\bigg), \tag{5}$$

$$I_{d_{i,j}} = \frac{\tau_{d_i}\left(e^{\chi_i} - 1\right)}{T}\bigg(-I_{p_i} - \frac{a_{0_i}(t_{0_i} - u_{i,j}T)}{\tau_{d_i}\left(e^{\chi_i} - 1\right)} + 1\bigg), \tag{6}$$

$$t_{0_i} = u_{i,j}T + \tau_{d_i} ln\left(\frac{R_{d_i}v_h}{(v_l + V_{F_{i,j}})R_{c_i}}\left(1 - e^{\kappa_i}\right) + 1\right),$$

$$\chi_i = \frac{u_{i,j}T - t_{0_i}}{\tau_{d_i}},\ a_{0_i} = \frac{v_l + V_{F_{i,j}}}{R_{d_i}}.$$

$$I_{p_i} = \frac{v_h}{R_{c_i}}\bigg(1 - e^{\kappa_i}\bigg),\ \kappa_i = \frac{t_d - u_{i,j}T}{\tau_{c_i}},$$

$$\lambda_i = \frac{t_d - t}{\tau_{c_i}},\ \phi_{i,j} = \frac{u_{i,j}T - t}{\tau_{d_i}},\ R_{d_i} = R_{0_l} + R_{L_i},$$

$$R_{c_i} = R_{0_h} + R_{L_i} + R_{ds},\ \tau_{c_i} = L_i/R_{c_i},\ \tau_{d_i} = L_i/R_{d_i},$$

where v_h and v_l, and R_{0_h} and R_{0_l} are the higher and lower open circuit voltages and series resistances (Ω) of two adjacent higher and lower SoC cells, respectively; $V_{F_{i,j}}$ is the forward voltage drop of diode $D_{i,j}$ parallel to MOSFET $Q_{i,j}$ (cf. Figure 1); τ_c and τ_d are time constants (s) for charging and discharging of inductor i, respectively; I_{p_i} is the peak inductor current at $t = u_{i,j}T$; t_d, t_{0_i} and T represent dead time, time instant at which inductor current is zero, and switching time period, respectively; duty cycle of $Q_{i,j}$ is denoted by $u_{i,j}$, and L_i represents the inductance of the inductor i (H); and R_{L_i}, R_{ds}, R_{c_i} and R_{d_i} represent resistances of inductor, on-state switching, and charging and discharging paths of inductor, respectively.

2.3. Power Losses of the ACBN

The model accounts for various power losses in the ACBN and includes both static and dynamic parameters of the network. The detailed model equations are taken from [22] and extended for a battery pack of N series-connected cells.

The power losses due to on-state resistances of MOSFETs, diodes, parasitic resistances of energy storage elements, and internal resistances of cells constitute the conduction losses, which are characterized as

$$P_{con} = \sum_{i=1}^{N-1}\sum_{j=1}^{2}\left[\mathcal{I}^2_{c_{i,j}}\tilde{R}_{c_i}u_{i,j} + \mathcal{I}^2_{d_{i,j}}\tilde{R}_{d_i}\left(\frac{t_{0_i} - u_{i,j}T}{T}\right)\right] + \sum_{n=1}^{N} I^2_{b_n}R_{0_n}, \tag{7}$$

$$\mathcal{I}^2_{c_{i,j}} = \frac{v_h^2}{TR^2_{c_i}}\left[\tau_{c_i}e^{\kappa_i}\left(\frac{4 - e^{\kappa_i}}{2}\right) + u_{i,j}T - t_d - \frac{3}{2}\tau_{c_i}\right],$$

$$\mathcal{I}^2_{d_{i,j}} = \frac{1}{T}\left[\tau_{d_i}I_{p_i}\left(\frac{I_{p_i}}{2} - a_{0_i}\right) + a^2_{0_i}\left(t_{0_i} - u_{i,j}T - \frac{3}{2}\tau_{d_i}\right) + e^{3\kappa_i}2a_{0_i}\tau_{d_i}\left(I_{p_i} + a_{0_i}\right)\right]$$

$$+\frac{1}{T}\left[-\tau_{d_i}e^{2\kappa_i}\left(\frac{I_{p_i}^2}{2}+\frac{a_{0_i}^2}{2}+a_{0_i}I_{p_i}\right)\right],$$

where P_{con} are the overall conduction power losses (W); $\mathcal{I}_{c_{i,j}}$ and $\mathcal{I}_{d_{i,j}}$ represent the effective RMS currents during charging and discharging modes, respectively; and $\tilde{R}_{c_i} = R_{c_i} - R_{0_h}$ and $\tilde{R}_{d_j} = R_{d_i} - R_{0_l}$.

The BBC is operated in discontinuous conduction mode, therefore, the switching losses in (8) only consider the power losses when MOSFETs are turned off

$$P_{t_f} = \frac{t_f}{2T}v_h\sum_{i=1}^{N-1}\sum_{j=1}^{2}I_{d_{i,j}}, \tag{8}$$

where t_f is the fall time.

The reverse recovery power loss associated with the body diode $D_{i,j}$ is

$$P_{D_{rr}} = \frac{t_{rr}^2}{2T}v_l\sum_{i=1}^{N-1}\sum_{j=1}^{2}\left(\frac{v_l + v_{F_{i,j}}}{L_i}\right). \tag{9}$$

During dead time both MOSFETs are off, however the inductor current keeps on flowing through the body diodes

$$P_{t_d} = \frac{t_d}{2T}\sum_{i=1}^{N-1}\sum_{j=1}^{2}\left(V_{F_{i,j}}I_{d_{i,j}}\right), \tag{10}$$

where P_{t_d} represents dead time power losses.

The model developed in this section will be used to design an NMPC for the ACBN in the subsequent section.

3. Nonlinear Model Predictive Control Design for the ACBN

The objective of this research work is to explore the impact of cell balancing on the range of an EV. According to the statistical analysis carried out

in section 4, it has been demonstrated that balancing aware NMPCs improve the range of an EV. However, unnecessarily prioritizing the cell balancing can increase the power losses in the ACBN. Therefore, we propose the following nonlinear programming problem (NLP)–transcribed using multiple-shooting method, which takes into account both the competing objectives–increased balancing speed and reduced power losses

$$\min_{\mathbf{x(k)},\mu(\mathbf{k})} J(\mathbf{x}(\mathbf{k}),\mu(\mathbf{k})), \tag{11}$$

$$J = \sum_{k=k_0}^{k_0+H_p}\left(\sum_{n=1}^{N} w_x \mathbf{e}_n^2(k) + w_p P_T(k)\right),$$

$$e_n(k) = x_n(k) - \bar{x}(k),\ \bar{x}(k) = \frac{1}{N}\sum_{n=1}^{N} x_n(k),$$

$$P_T(k) = P_{con}(k) + P_{tf}(k) + P_{D_{rr}}(k) + P_{t_d}(k),$$

subject to

$$\mathbf{x}(\mathbf{k}+\mathbf{1}) - \mathbf{f}(\mathbf{x}(\mathbf{k}),\mu(\mathbf{k})) = 0, \tag{11a}$$

$$\mathbf{x}(k_0) = \mathbf{x}_{k_0}, \tag{11b}$$

$$\mu(\mathbf{k}) \in \mathcal{U}, \tag{11c}$$

$$\mathbf{x}(\mathbf{k}) \in \mathcal{X}, \tag{11d}$$

$$\mu_{i,1}^T(k)\mu_{i,2}(k) = 0, \tag{11e}$$

where $\mu(\mathbf{k}) = \mathbf{u}(\mathbf{k}) - t_d/T$; H_p is the prediction horizon (s); $w_x, w_p \in \Re^+$ are the weights for SoC balancing and total power losses (P_T), respectively; $\mathbf{x}_{k_0}$ is the initial state vector at the start of the optimization problem; $\mu_{i,1}^T = \begin{bmatrix}\mu_{1,1} & \mu_{2,1} & \dots & \mu_{(N-1),1}\end{bmatrix}$ and $\mu_{i,2}^T = \begin{bmatrix}\mu_{1,2} & \mu_{2,2} & \dots & \mu_{(N-1),2}\end{bmatrix}$; and the sets

$\mathcal{U}$ and $\mathcal{X}$ in (11c) and (11d), respectively are given as

$$\mathcal{U} = \left\{ \mu_{i,j} \in \Re^{+} \middle| 0 \leq \mu_{i,j} \leq u_{max} - \frac{t_d}{T} \right\},$$
$$\mathcal{X} = \left\{ x_n \in \Re^{+} \middle| x_{min} \leq x_n \leq x_{max} \right\},$$

where x_{min} and x_{max} are the minimum and maximum SoC levels of the cell n, and u_{max} represents the maximum value of the MOSFET's duty cycle. The equality constraint in (11e) makes sure that both the MOSFETs of any BBC are not turned on simultaneously, eventually preventing short circuit in the ACBN.

The cost function J in (11) has two terms: the first term is the sum of the squares of the difference of individual SoC level of a cell and the average SoC levels of all cells, and the second term represents the total power losses in the ACBN. If w_p is kept small then the NMPC expedites balancing of the SoC levels of the cells, whereas, for larger values of w_p the controller gives more weightage to P_T and tries to minimize the power losses. The NMPC solves the NLP in (11) at every time instant and yields optimal values of states and control inputs–$\mathbf{x}_{opt}(k)$ and $\mu_{opt}(k)$ for interval $[k_0,\ k_0 + H_p]$. However, the closed-loop input for the interval is $\mu^* := \mu_{opt}(k_0)$, whereas, the remaining control actions are discarded.

3.1. Stability of the Closed-Loop System

The stability of the closed-loop system is derived by exploiting the dynamics of the ACBN in section 2 and constraints of the NLP in (11).

Consider the following Lyapunov functional

$$V = \mathbf{e}^T \mathbf{e} + w_p P_T, \tag{12}$$

$$\mathbf{e}^T = \begin{bmatrix} e_1 & e_2 & \dots & e_N \end{bmatrix}.$$

The time derivative of V in (12) is given as

$$\begin{aligned} \dot{V} &= \mathbf{e}^T\dot{\mathbf{e}} + \dot{\mathbf{e}}^T\mathbf{e} + w_p\dot{P}_T, \\ &= 2\left(e_1\dot{e}_1 + \sum_{n=2}^{N-1} e_n\dot{e}_n + e_N\dot{e}_N\right) + w_p\dot{P}_T. \end{aligned} \tag{13}$$

Depending upon the SoC levels of two adjacent cells, the NMPC turns the MOSFETs on by respecting (11e). In a string of N series connected cells there can be N^N combinations based on cells' initial SoC levels. However, for stability analysis only two extreme cases are considered here–the first case assumes that $x_1 > x_2 > \ldots > x_N$, whereas the second case considers $x_1 < x_2 < \ldots < x_N$. Employing (1) in (13), the stability of the closed-loop system is established for both the cases using the Lyapunov theory.

3.1.1. Stability Analysis for Case-I ($x_1 > x_2 > \ldots > x_N$)

In this case only first MOSFET of each buck-boost converter is turned-on, while the second MOSFET stays off, therefore $\mu_{i,2}(k) = \mathbf{0}$ in (11e), and for an inductor L_i, $I_{d_{i,2}} = I_{c_{i,2}} = 0$. Consequently, by assuming that all the cells have capacity η, the expressions for $\dot{e}_1$, $\dot{e}_n$ and $\dot{e}_N$ can be written as

$$\begin{aligned} \dot{e}_1 &= \frac{1}{N\eta}\left[(N-1)\, I_{c_{1,1}} - \Pi_1 - I_{d_{(N-1),1}}\right], \\ \dot{e}_n &= \frac{1}{N\eta}\left[N\left(I_{c_{n,1}} + I_{d_{(n-1),1}}\right) - I_{c_{1,1}} - I_{d_{(N-1),1}} - \Pi_1\right], \\ \dot{e}_N &= \frac{1}{N\eta}\left[(N-1)\, I_{d_{(N-1),1}} - \Pi_1 - I_{c_{1,1}}\right], \end{aligned} \tag{14}$$

where $\Pi_1 = \sum_{n=2}^{N-1}\left(I_{c_{n,1}} + I_{d_{(n-1),1}}\right)$.

With the choice of parameters, given in section 4, and by assuming same resistance for charging (R_{c_i}) and discharging (R_{d_i}) paths of inductor, the magnitudes of both $I_{c_{i,j}}$ and $I_{d_{i,j}}$ are same, and $|I_{c_{i,j}}| = |I_{d_{i,j}}| \leq I^*$. After using these results in (14), $\dot{e}_n = 0$ and $\Pi_1 = 0$ (same number of charging and discharging currents). In Case-I $e_1 > 0$ and $e_N < 0$, therefore, the time derivative of the Lyapunov functional in (13) becomes

$$\dot{V} \leq -\frac{2I^*}{\eta}\Big(|e_1| + |e_N|\Big) + w_p \dot{P}_T. \tag{15}$$

By proper choice of w_p, $\dot{V} \leq 0$, and by using invariant set theorem it can be shown that SoC level of each cell converges to the average SoC level.

3.1.2. Stability Analysis for Case-2 ($x_1 < x_2 < \ldots < x_N$)

In this case only second MOSFET of each buck-boost converter is turned-on, therefore $\mu_{i,1} = \mathbf{0}$ in (11e), and $I_{d_{i,1}} = I_{c_{i,1}} = 0$. The time derivatives of $\dot{e}_1$, $\dot{e}_n$ and $\dot{e}_N$ can be expressed as

$$\begin{aligned}
\dot{e}_1 &= \frac{1}{N\eta}\Big[(N-1)\, I_{d_{1,2}} - \Pi_2 - I_{c_{(N-1),2}}\Big], \\
\dot{e}_n &= \frac{1}{N\eta}\Big[N\Big(I_{c_{(n-1),2}} + I_{d_{n,2}}\Big) - I_{d_{1,2}} - I_{c_{(N-1),2}} - \Pi_2\Big], \\
\dot{e}_N &= \frac{1}{N\eta}\Big[(N-1)\, I_{c_{(N-1),2}} - \Pi_2 - I_{d_{1,2}}\Big],
\end{aligned} \tag{16}$$

where $\Pi_2 = \sum_{n=2}^{N-1}\Big(I_{c_{(n-1),2}} + I_{d_{n,2}}\Big)$.

After considering the magnitudes of charging and discharging currents, and using the fact that $e_1 < 0$ and $e_N > 0$, same result as given by (15) is obtained. Using the above analysis, a similar conclusion can be drawn for the stability of the closed-loop system for any initial SoC distribution.

4. Results and Discussion

The discussion of the results will be distributed into three main categories. Firstly, the results of NMPC and its subsequent impact on ACBN performance will be discussed. Secondly, the discussion will be about statistical analysis of the impact of input parameters–cost function, initial SoC configuration, and drive cycles, on the performance metrics–range, balancing time, and power losses. The statistical tools used in this research work are the analysis of variance (ANOVA) and multivariate (ANOVA). Finally, the system-level impact of employing NMPC for ACB in terms of range extension will be covered. Moreover, it is pertinent to mention that the current framework provided in this work to analyze the ACBN performance can easily be extended to incorporate other physical variables. For instance, the thermal and aging models can be integrated with the current ACBN model. This in turn will allow to expand the NMPC to be thermal and health aware by including more terms in its cost function.

Along with the cost function considered in (11), we have also incorporated two more. For brevity, we will simply list them while omitting the full NMPC formulation, which remains unchanged. Note that from here onwards, we are going to refer the cost function in (11) as J_3. The other two cost functions are given as

$$J_1 = \sum_{k=k_0}^{k_0+H_p} \Big(-w_x (\min(\mathbf{x}(\mathbf{k})))^2 + w_p P_T(k) \Big), \tag{17}$$

$$J_2 = \sum_{k=k_0}^{k_0+H_p} \Big(w_x (\max(\mathbf{x}(\mathbf{k})) - \min(\mathbf{x}(\mathbf{k})))^2 + w_p P_T(k) \Big), \tag{18}$$

$$\min(\mathbf{x}) = -\frac{1}{w_s} log \left(\sum_{n=1}^{N} \exp(-w_s x_n) \right),$$

$$\max(\mathbf{x}) = \frac{1}{w_s} log\left(\sum_{i=1}^{N} \exp(w_s x_i)\right),$$

, where w_s is the scaling parameter. The values of w_p, w_p, w_s and H_p are determined after performing sensitivity analysis and evaluating the performance in terms of balancing time, power losses, and computational burden. After the analysis, the values are set as $w_p = 10^{-4}$, $w_x = 10$, $w_s = 100$, and $H_p = 10$. The term representing the power losses is similar in all the cost functions, while the balancing term is different. In J_1 the least SoC level is maximized, whereas J_2 minimizes the difference between maximum and minimum SoC. In order to improve the feasibility of the solution of the optimal control problem, smooth approximations of $\min(x)$ and $\max(x)$ are used.

The closed-loop implementation employing NMPC for ACBN is illustrated in Figure 1. Taking in the values of $\mathbf{x}$, the NMPC block calculates the duty cycles for the BBCs to balance the cells' SoC levels. Figure 1 demonstrates the control implementation scheme for a string of N series-connected cells, however, the simulations are performed for $N = 12$ cells. This number of cells represents a case study for a low- to medium-powered EV bike, wherein twelve serially connected cells are sufficient to provide a voltage of up to 40 V. Moreover, for simulation purposes, all cells are considered to be LG 18650HG2 type (cf. [25]), and the cells' and ACBN nominal parameters are given in Table 2.

The NLP in (11), (17), and (18), is implemented in Simulink using the CasADi framework and solved using the interior point optimizer (Ipopt) algorithm. Moreover, the Euler method is used to discretize the mathematical model in the NMPC and overall closed-loop system, with a time step of

10 s. The constraints on the input and states are $u_{\max} = 0.4$, $x_{\min} = [0.05, \ldots, 0.05]^\top \in \mathbb{R}^{12}$, $x_{\max} = [0.95, \ldots, 0.95]^\top \in \mathbb{R}^{12}$, with prediction horizon $H_p = 20$ s. All the simulations were performed on a computer with an Intel Core i7-1065G7, 1.3 GHz, 10^{th}-generation processor; 16 GB RAM; running Windows 11 Home (64-bit). Moreover, under these computational settings, the optimizer took an average of 1.3 s to solve an optimization problem, with a convergence rate of -0.0054 s^{-1}. Finally, the memory footprint is estimated to be < 50 KB. This is approximated as follows: $N_{\text{var}} = \underbrace{n_x}_{\text{Initial State } X_0} + \underbrace{N_p}_{\text{Horizon}} \times \left(\underbrace{n_u}_{\text{Controls } U_k} + \underbrace{n_x}_{\text{Next State } X_{k+1}} \right)$, where N_{var} represents the total number of decision variables, and values of H_p, n_u, and n_x are 2, 22, and 12, respectively. Consequently, 80 decision variables, along with consideration of double-precision storage and sparse solver overhead for Hessian and Jacobian matrices, approximately amounts to memory footprints of < 50 KB.

All of the above-mentioned cost functions in various NMPC formulations are balancing-aware; however, they yield different performance metrics. Similarly, the range achieved by EV is calculated using the following:

$$\text{Range} = \int_0^{t_{sim}} v_{DC}(t)dt, \tag{19}$$

where v_{DC} is the velocity profile of drive cycles, and t_{sim} is the instant when SoC of any battery cell reaches 10%. Moreover, the balancing time t_b is the time when the standard deviation of the cells' SoC is $\sigma(\mathbf{x}(k)) = 0.02$. At this point, it is crucial to mention that t_{sim} is predominately dictated by the EV powertrain's parameters and battery characteristics. This is because I_e, which serves as an input to the battery pack, is obtained after giving

v_{DC} as input to the EV powertrain simulator. Consequently, all the vehicle- and battery-related characteristics, which are defined in the simulator, are reflected in I_e, which governs the rate of SoC drop in a pack. Similarly, to quantify EV range extension as a result of ACB, we first need to set a baseline scenario. Since in this work we are interested in range enhancement solely due to ACB, we consider the no-balancing (NB) scenario as a baseline. Subsequently, for any drive cycle, the difference in ranges achieved by NMPC-based ACB and NB is quantified as range extension.

Table 2: Nominal model parameters for simulations

Parameter	**Value**	**Parameter**	**Value**
T	20 μs	t_d	2 μs
V_F	0.3 V	R_{ds}	5.3 mΩ
t_f	8 ns	t_{rr}	28 ns
R_L	0.01 Ω	L	6 μH
R_{0_i}	0.025 Ω	η_{nom}	10800 As

Figures 3–5 show the outcomes of ACBN against the current of FUDS driving profile, depicted in Figure 2, for cost functions J_1–J_3. The initial SoC levels of cells are given by $\mathbf{x}(0) = [\,0.7\ 0.7\ 0.7\ 0.7\ 0.8\ 0.8\ 0.8\ 0.8\ 0.9\ 0.9\ 0.9\ 0.9\,]$. As expected, in all three scenarios–see Figures 3a, 4a, and 5a the cells' SoC levels were ultimately equalized, but with varying t_b of 79600 s, 5770 s, and 5600 s for J_1, J_2, and J_3, respectively. Moreover, it can be seen from Figures 3b, 4b and 5b that even after the balancing criterion is met, $\sigma(\mathbf{x}(k))$ continues to drop and almost reaches zero for J_2 and J_3; on the other hand,

a small difference exists in SoC levels for J_1. Nevertheless, in all of the scenarios, the balancing criteria is met and sustained, demonstrating the robust performance of the controller. In continuation, Figures 3c, 4c, 5c, and Figures 3d, 4d, 5d depict the control actions and corresponding balancing currents, respectively. The results indicate that for all cost functions the controller remains involved even past when the balancing criteria are met, subsequently generating balancing currents with diminishing magnitude to equalize cells' SoC levels.

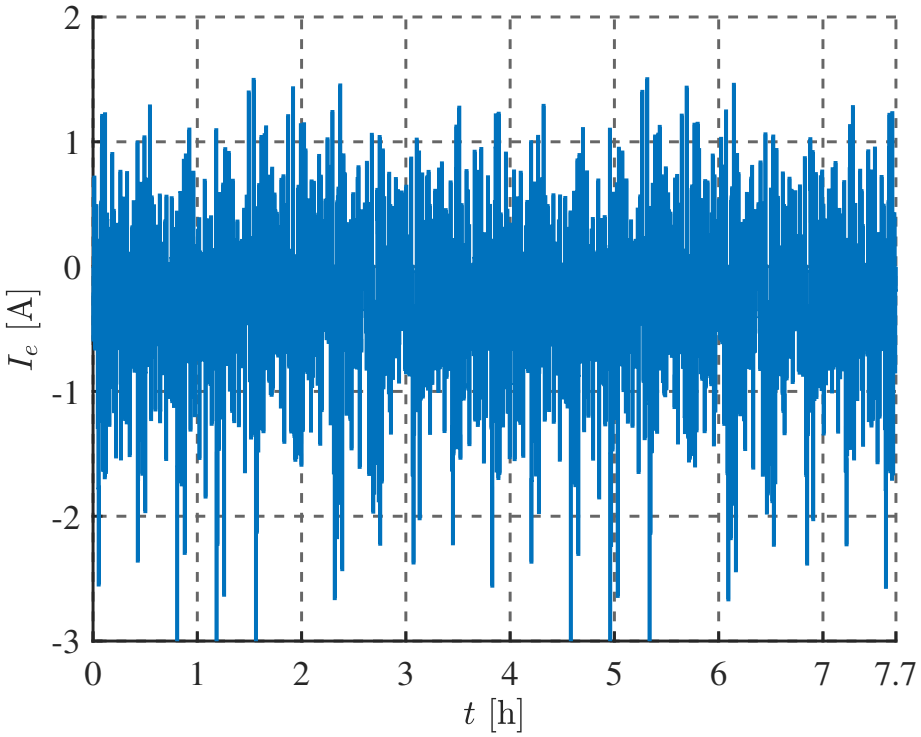

Figure 2: Current profile for FUDS drive cycle.

In order to conduct statistical analysis to quantify the impact of closed-loop parameters, we have performed ACB and collected data against the

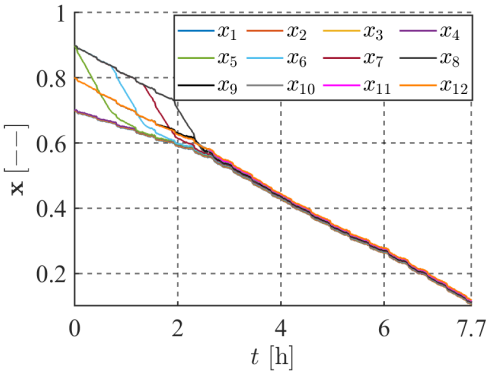

(a) SoC levels of the cells.

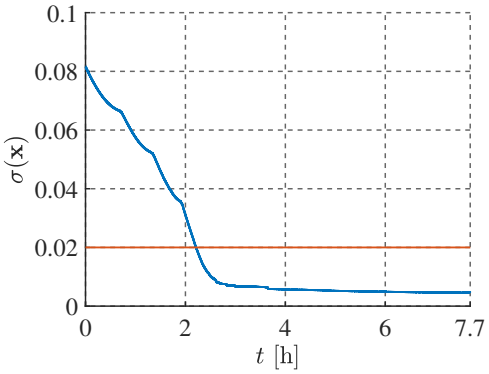

(b) Standard deviation of cells SoC.

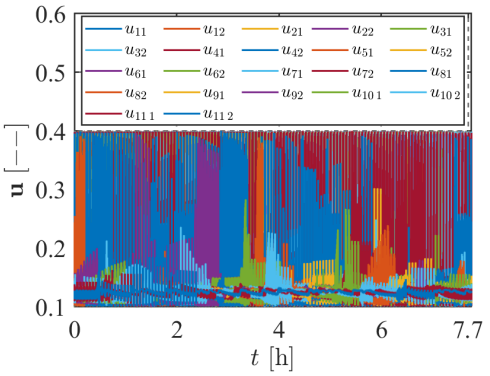

(c) Duty cycles (control inputs).

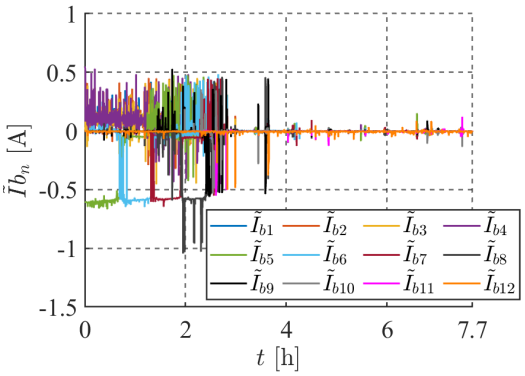

(d) Cells currents, $\tilde{I}b_n = I_{b_n} - I_e$.

Figure 3: NMPC results with cost function J_1 and FUDS drive cycle.

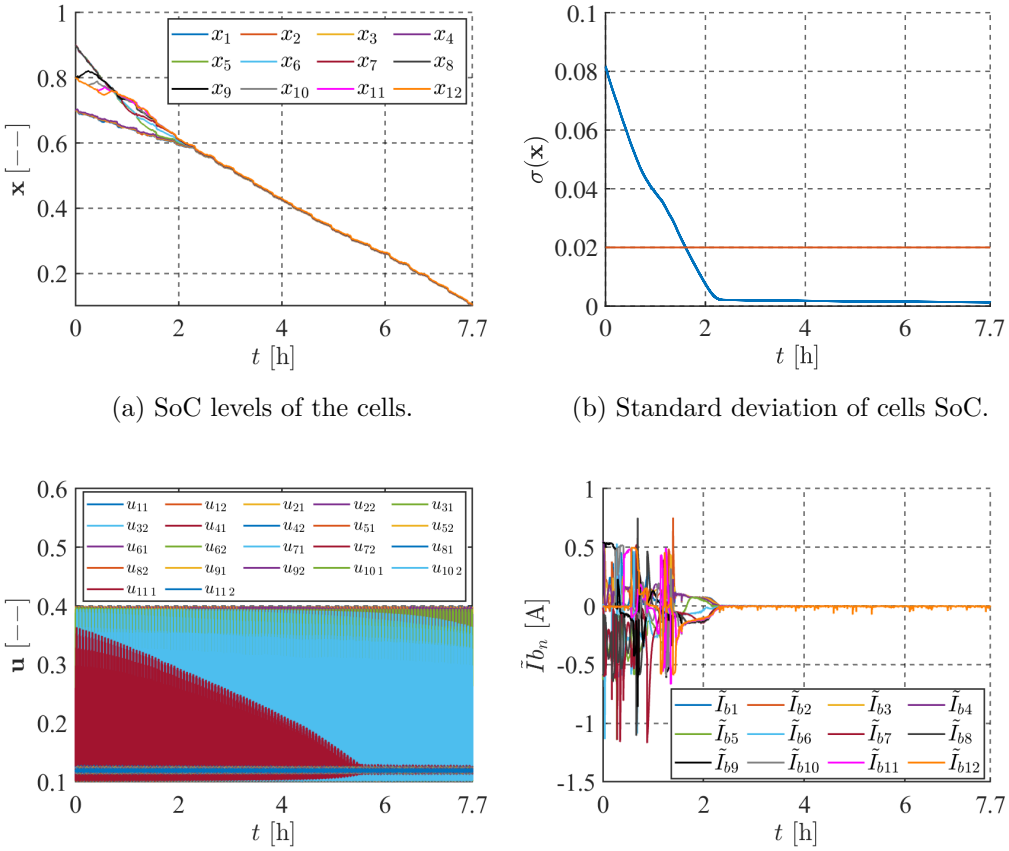

(a) SoC levels of the cells.

(b) Standard deviation of cells SoC.

(c) Duty cycles (control inputs).

(d) Cells currents.

Figure 4: NMPC results with cost function J_2 and FUDS drive cycle.

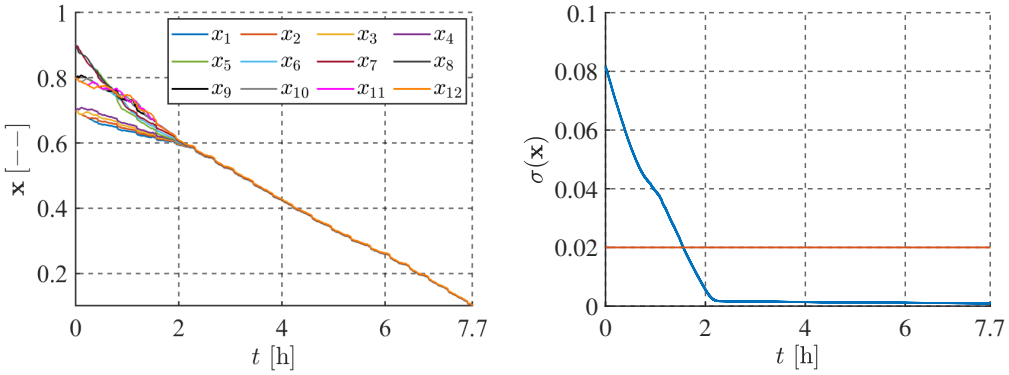

(a) SoC levels of the cells.

(b) Standard deviation of cells SoC.

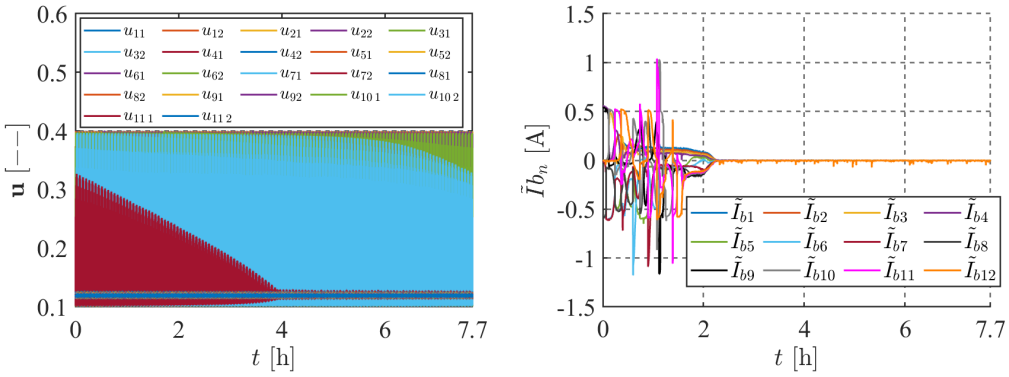

(c) Duty cycles (control inputs).

(d) Cells currents.

Figure 5: NMPC results with cost function J_3 and FUDS drive cycle.

following sets. $\mathcal{D} = \{$FHDS (D_1), FUDS (D_2), FUDS Fast (D_3), NEDC (D_4), US06 (D_5), US06 City Cycle (D_6), US06 Highway Cycle (D_7)$\}$ is the set of standardized drive cycles [26]; moreover, the set of initial SoC configuration ($\mathcal{X}_{\text{conf}}$) is defined as follows: first we distribute our set of initial vector i.e, $\mathbf{x}$ into 3 distinct blocks as: $b_1 = [0.9, 0.9, 0.9, 0.9]$, $b_2 = [0.8, 0.8, 0.8, 0.8]$, and $b_3 = [0.7, 0.7, 0.7, 0.7]$, subsequently, $\mathcal{X}_{\text{conf}} = \{[b_\varphi, b_\vartheta, b_\varrho] \mid \varphi, \vartheta, \varrho \in \{1, 2, 3\}\}$; and finally $\mathcal{J} = \{J_1,\ J_2\ J_3\}$ is the set of cost functions. Subsequently, the total number of simulations conducted to collect data can be defined as the cartesian product of the above three sets i.e, $\mathcal{D} \times \mathcal{X}_{\text{conf}} \times \mathcal{J}$–567 simulations in total.

$\mathcal{N}$-way ANOVA is a statistical method that aids in understanding the variance in a single output/dependent variable as a result of varying the $\mathcal{N}$ input/independent variables, which have different levels or groups. For instance, in this work, $\mathcal{D}$ has 7 groups. Similarly, MANOVA expands the $\mathcal{N}$-way ANOVAs capabilities by allowing it to incorporate and analyze more than one output variable. The outcomes of these analyses are usually characterized by the F-ratio, which is a dimensionless quantity and is defined as the ratio of variance between groups to the variance within groups [27]; the summary for these scores is provided in Table 3 for the reader's convenience. A higher F-ratio implies a statistically significant impact of input variables on outputs. With an F-ratio of 145.38, the MANOVA analysis shows that the drive cycles have the most impact on the variations of the outputs; this is followed by initial SoC configuration and cost function, with F-ratios of 33.517 and 32.681, respectively. Similarly, in terms of impact on individual output factors, ANOVA reveals that drive cycle is the strongest cause behind

the variations in range and $\bar{P}_T$, achieving 15954 and 52777, respectively, as F-ratios. On the other hand, initial SoC configuration has the least impact on the variation in $\bar{P}_T$ and cost function minimally impacts range, with F-ratios of 40.344 and 31.921, respectively. Likewise, for t_b, ANOVA shows that the prominent source of influence behind its variance is the cost function, with an F-ratio of 105.2, whereas the drive cycle has the least impact, with F-ratios of 2.08. These findings stress the need to take into account dynamic driving behaviors, initial cell conditions, and appropriate choice of cost function in the design of ACB techniques to improve balancing performance and extend the range of the EV.

Independent Variable	**MANOVA F-ratio**	**ANOVA Range F-ratio**	**ANOVA $\bar{P}_T$ F-ratio**	**ANOVA t_b F-ratio**
Cost function	32.681	31.921	84.287	105.2
Drive cycle	145.38	15 954	5 2777	2.08
Initial SoC	33.517	637	40.344	83.865

Table 3: Summary of F-ratios for ANOVA and MANOVA analysis to quantify the impact of certain parameters on EVs range and ACBN performance.

Finally, this paragraph will engage the discussion regarding the system-level manifestation in terms of range as a consequence of ACB. Moreover, it is pertinent to mention that in Figures 6a, 6b, and 6c, the quantities shown are averaged over all the set $\mathcal{X}_{\text{conf}}$. Upon closer scrutiny of Figure 6a, it becomes

evident that irrespective of the cost function, the NMPC based ACB yields increased range as compared to the NB case. Moreover, across individual drive cycles, J_2 consistently demonstrates superior performance compared to other cost functions: it has yielded a maximum range extension of 20% in D_3 (J_1 and NB attained ranges of 161 km and 136 km, respectively), and a minimum range extension of 13% in D_5 (with ranges of 149.4 km and 134 km for J_1 and NB, respectively). Similarly, J_1 has yielded a maximum and minimum range extension of 18.4% and 11.5% in D_3 and D_5 respectively. Table 4 reports the maximum and minimum range achieved by each cost function and its corresponding drive cycle. Moreover, all these numbers for range extension are reported for just a single EV executing a single drive cycle. Consequently, these numbers can easily scale up to millions of kilometers considering a large number of EVs running thousands of drive cycles over their lifespan.

In a similar vein, concerning $\bar{P}_T$, as depicted in Figure 6b, J_1 incurs the highest loss of 1.19 W in D_5, whereas it records the lowest loss of 0.13 W in D_4. Similarly J_2 demonstrates the maximum and minimum losses of 1.22 W and 0.13 W in D_5 and D_4 respectively; and for J_3, the values are 1.23 W and 0.13 W, respectively. All the cost functions yield maximum value of $\bar{P}_T$ in D_5, which is the most demanding drive cycle with high magnitude of I_e; whereas D_4–exhibiting a relatively smooth I_e profile and low current magnitude–yields the least value of $\bar{P}_T$ for all cost functions– see Table 4.

Finally, similar analysis regarding t_b is demonstrated in Figure 6c. It is from the Figure that J_3 yields the least balancing time in almost all the drive cycles, except for D_5 and D_7, where J_2 dominates J_3 in terms of balancing

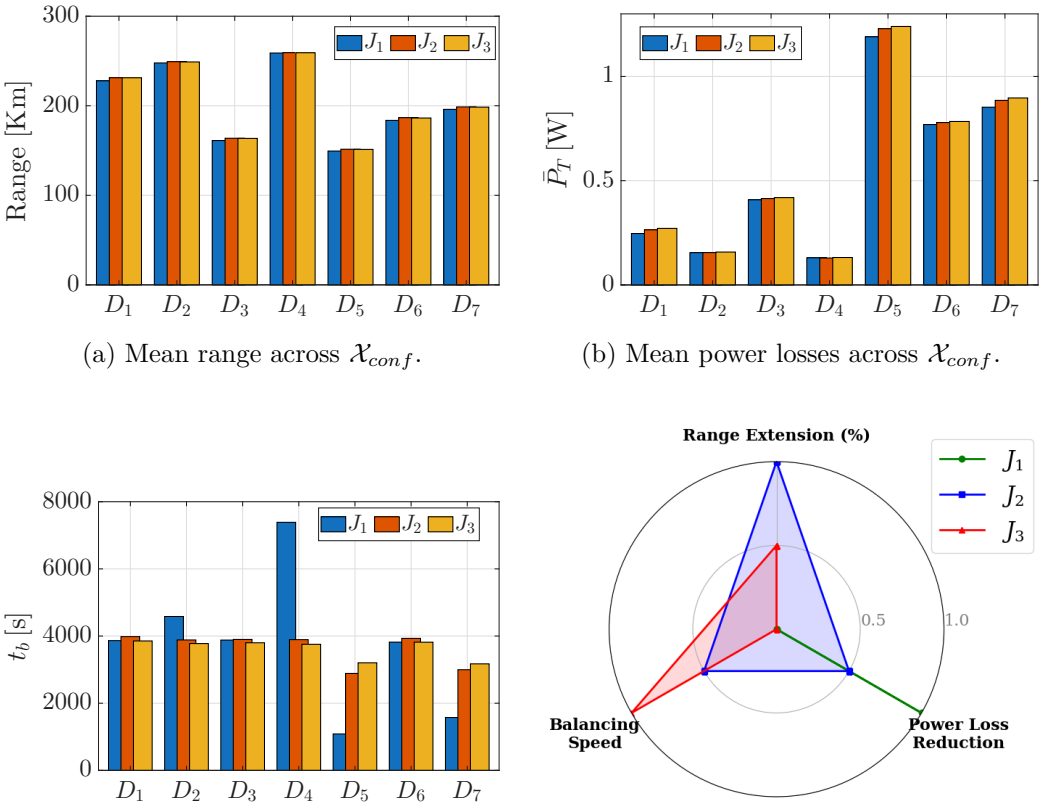

(a) Mean range across $\mathcal{X}_{conf}$.

(b) Mean power losses across $\mathcal{X}_{conf}$.

(c) Mean balancing time across $\mathcal{X}_{conf}$.

(d) Relative performance of cost functions

Figure 6: Statistics of NMPC-based ACBN performance metrics (Range,$\bar{P}_T$ and t_b) for all the drive cycles in $\mathcal{D}$.

speed. J_3 exhibits the maximum and minimum improvement in t_b of 96.8% and 0.25% with respect to J_1, in D_4 and D_1, respectively. However, it is interesting to note that J_1 achieves competitive performance in aggressive driving regimes such as D_5, D_6, and D_7; whereas for mild drive cycles, i.e., D_4, its performance deteriorates, with t_b reaching the value of 7386 s.

Table 4: Comparison of maximum and minimum range, power loss, and balancing Time for each cost function along with the corresponding drive cycle.

Cost Function	**Range** (km)		**Avg Power Loss (W)**		**Balancing Time** t_b **(s)**	
	Max	**Min**	**Max**	**Min**	**Max**	**Min**
J_1	258.9 (D_4)	149.4 (D_5)	1.19 (D_5)	0.13 (D_4)	7386 (D_4)	1084 (D_5)
J_2	259.2 (D_4)	151.4 (D_5)	1.22 (D_5)	0.12 (D_4)	3982 (D_1)	2887 (D_5)
J_3	259.1 (D_4)	151.3 (D_5)	1.2 (D_5)	0.13 (D_4)	3853 (D_1)	3172 (D_7)
NB	220 (D_4)	134 (D_5)	1.15 (D_5)	0.12 (D_7)	–	–

In summary, after taking the average over all drive cycles, J_2 has demonstrated a 16.26% range extension; whereas J_3 and J_1 have yielded the values of 16% and 14.9%, respectively. And for average power losses, J_3, incurred the maximum loss of 0.55 W, followed by J_2, and J_1, with the values of 0.54 and 0.53 W, respectively. Finally, J_1 has the maximum value of $t_b = 3741$ s, while J_3 has the least value of $t_b = 3628$ s. This analysis suggests that J_2 is the preferred cost function if range extension is the desired performance criterion and J_3 is appropriate for achieving faster balancing times; moreover, J_1, with the least power losses, proves to be the best option if efficiency of the ACBN is critical. All in all, J_2 has shown an intermediate overall performance–yielding better balancing speed and range and balancing efficiency as compared to J_3 and J_1. The relative performance and selection

criteria of each cost for different performance metrics are demonstrated in Figure 6d.

5. Conclusion and Future work

To address the concern of EV range anxiety, this work employs ACB under the NMPC framework. In this respect, first a high-fidelity mathematical model of ACBN comprising N serially connected cells arranged in adjacent cell-cell topology is provided. Building on that, an NMPC problem is formulated and subsequently solved for $N = 12$ cells–representing a case study for an EV bike. Furthermore, conclusive arguments are provided to demonstrate the stability of the above generalized problem using Lyapunov-based analysis. Simulations were performed by considering various real driving scenarios, initial SoC conditions, and three distinct NMPC formulations in terms of cost functions. The results demonstrated that under NMPC-based ACB, an average of 28.9 km of range extension can be achieved. Subsequently, statistical analysis were performed using MANOVA, which quantified the impact of NMPC cost functions, initial SoC configurations, and drive cycles on ACBN performance metrics.

The future work aims to incorporate the thermal and aging model into the existing electrical model of the cell. This will allow us to include other performance metrics such as thermal and health regulation and evaluate the impact of ACB on them. Moreover, machine learning algorithms will be applied to the data collected in this work to dynamically switch between different cost functions of NMPC in the face of diversified driving conditions.

Acknowledgements

The authors would like to thank Pakistan Science Foundation for funding this research through Grant Number: PSF-CRP/TUBITAK-IV/EV/C-COMSATS (26).

References

[1] E. Ferrero, S. Alessandrini, A. Balanzino, Impact of the electric vehicles on the air pollution from a highway, Appl. Energy 169 (2016) 450–459. doi:10.1016/j.apenergy.2016.01.098.

[2] N. Khan, C. A. Ooi, A. Alturki, M. Amir, Shreasth, T. Alharbi, A critical review of battery cell balancing techniques, optimal design, converter topologies, and performance evaluation for optimizing storage system in electric vehicles, Energy Rep. 11 (2024) 4999–5032. doi:10.1016/j.egyr.2024.04.041.

[3] J. C. Geromel, Model Predictive Control, in: Differential Linear Matrix Inequalities, Springer, Cham, Switzerland, 2023, pp. 207–231. doi:10.1007/978-3-031-29754-0_8.

[4] P. T. Abadie, D. J. Docimo, A framework for analysis of lithium-ion battery pack balancing including cell parameter heterogeneity, IFAC-PapersOnLine 55 (37) (2022) 726733. doi:https://doi.org/10.1016/j.ifacol.2022.11.268.

[5] J. Chen, Z. Zhou, Z. Zhou, X. Wang, B. Liaw, Impact of battery cell

imbalance on electric vehicle range, Green Energy and Intelligent Transportation 1 (3) (2022) 100025. doi:10.1016/j.geits.2022.100025.

[6] B. O. Varga, A. Sagoian, F. Mariasiu, Prediction of Electric Vehicle Range: A Comprehensive Review of Current Issues and Challenges, Energies 12 (5) (2019) 946. doi:10.3390/en12050946.

[7] J. Liu, Y. Chen, H. K. Fathy, Nonlinear Model-Predictive Optimal Control of an Active Cell-to-Cell Lithium-Ion Battery Pack Balancing Circuit, IFAC-PapersOnLine 50 (1) (2017) 14483–14488. doi:10.1016/j.ifacol.2017.08.2297.

[8] D. Flessner, J. Chen, G. Xiong, Reinforcement Learning-Based Event-Triggered Active-Battery-Cell-Balancing Control for Electric Vehicle Range Extension, Electronics 13 (5) (2024) 990. doi:10.3390/electronics13050990.

[9] F. S. J. Hoekstra, H. J. Bergveld, M. C. F. Donkers, Range Maximisation of Electric Vehicles through Active Cell Balancing using Reachability Analysis, in: 2019 American Control Conference (ACC), IEEE, pp. 10–12. doi:10.23919/ACC.2019.8814748.

[10] F. S. J. Hoekstra, L. A. W. Ribelles, H. J. Bergveld, M. C. F. Donkers, Real-Time Range Maximisation of Electric Vehicles through Active Cell Balancing using Model-Predictive Control, in: 2020 American Control Conference (ACC), IEEE, pp. 01–03. doi:10.23919/ACC45564.2020.9147614.

[11] F. S. J. Hoekstra, H. J. Bergveld, M. C. F. Donkers, Optimal Control of Active Cell Balancing: Extending the Range and Useful Lifetime of a Battery Pack, IEEE Trans. Control Syst. Technol. 30 (6) (2022) 2759–2766. doi:10.1109/TCST.2022.3161764.

[12] J. Chen, A. Behal, C. Li, Active Cell Balancing by Model Predictive Control for Real Time Range Extension, in: 2021 60th IEEE Conference on Decision and Control (CDC), IEEE, pp. 14–17. doi:10.1109/CDC45484.2021.9682869.

[13] J. Chen, A. Behal, Z. Li, C. Li, Active Battery Cell Balancing by Real-Time Model Predictive Control for Extending Electric Vehicle Driving Range, IEEE Trans. Autom. Sci. Eng. (2023) 1–13doi:10.1109/TASE.2023.3291679.

[14] V. Azimi, A. Allam, S. Onori, Extending Life of Lithium-Ion Battery Systems by Embracing Heterogeneities via an Optimal Control-Based Active Balancing Strategy, IEEE Trans. Control Syst. Technol. 31 (3) (2022) 1235–1249. doi:10.1109/TCST.2022.3215610.

[15] A. Pozzi, M. Zambelli, A. Ferrara, D. M. Raimondo, Balancing-Aware Charging Strategy for Series-Connected Lithium-Ion Cells: A Nonlinear Model Predictive Control Approach, IEEE Trans. Control Syst. Technol. 28 (5) (2020) 1862–1877. doi:10.1109/TCST.2020.2995308.

[16] M. Azmat Ullah, A. Ahmed, A. A. Uppal, Q. Ahmed, Nmpc-based performance evaluation of active balancing networks of li-ion batteries

for overnight ev charging, IEEE Access 13 (2025) 136016–136026. doi:10.1109/ACCESS.2025.3594129.

[17] J. V. Barreras, R. de Castro, Y. Wan, T. Dragicevic, A Consensus Algorithm for Multi-Objective Battery Balancing, Energies 14 (14) (2021) 4279. doi:10.3390/en14144279.

[18] J.-C. M. Lin, Development of a globally active balance module with range extension effect, IET Electr. Syst. Transp. 7 (2) (2017) 154–160. doi:10.1049/iet-est.2016.0004.

[19] X. Lu, C. Wang, Fuzzy Equalization Strategy Based on Multilayer Circuits, JERR (2022) 76–88doi:10.9734/jerr/2022/v22i917566.

[20] T. Rüther, M. Schamel, C. Plank, F. Schomburg, F. Röder, M. A. Danzer, Cell-to-cell variation beyond parameter analysis — Identification and correlation of processes in Lithium-Ion Batteries using a combined distribution of relaxation times analysis, J. Power Sources 587 (2023) 233677. doi:10.1016/j.jpowsour.2023.233677.

[21] S. B. Javed, A. A. Uppal, M. R. Azam, K. Shehzad, Q. Ahmed, Model-Based Quantitative Analysis of a Capacitive Cell Balancing Technique using SoC Estimator, in: 2022 IEEE Conference on Control Technology and Applications (CCTA), IEEE, pp. 23–25. doi:10.1109/CCTA49430.2022.9966110.

[22] S. B. Javed, A. A. Uppal, M. R. Azam, Q. Ahmed, Model-based quantitative analysis of power losses aware active cell balancing networks

with load, IEEE Transactions on Transportation Electrification (2024) 1–1doi:10.1109/TTE.2024.3455767.

[23] A. A. Uppal, S. B. Javed, Q. Ahmed, Power Losses Aware Nonlinear Model Predictive Control Design for Active Cell Balancing, IEEE Control Syst. Lett. 7 (2023) 3705–3710. doi:10.1109/LCSYS.2023.3342550.

[24] N. Ghaeminezhad, Q. Ouyang, X. Hu, G. Xu, Z. Wang, Active cell equalization topologies analysis for battery packs: A systematic review, IEEE Transactions on Power Electronics 36 (8) (2021) 9119–9135. doi:10.1109/TPEL.2021.3052163.

[25] N. Campagna, V. Castiglia, R. Miceli, R. A. Mastromauro, C. Spataro, M. Trapanese, F. Viola, Battery models for battery powered applications: A comparative study, Energies 13 (16) (2020). doi:10.3390/en13164085.
URL https://www.mdpi.com/1996-1073/13/16/4085

[26] B. M. Geller, T. H. Bradley, Analyzing Drive Cycles for Hybrid Electric Vehicle Simulation and Optimization, J. Mech. Des. 137 (4) (2015) 041401. doi:10.1115/1.4029583.

[27] A. García-Pérez, Approximations for F-tests which are ratios of sums of squares of independent variables with a model close to the normal, Test 17 (2) (2008) 350–369. doi:10.1007/s11749-006-0036-4.

[28] S. Shrestha, B. Baral, M. Shah, S. Chitrakar, B. P. Shrestha, Measures

583 to resolve range anxiety in electric vehicle users, Int. J. Low-Carbon
584 Technol. 17 (2022) 1186–1206. doi:10.1093/ijlct/ctac100.

585 [29] H. Wang, M. Rasheed, R. Hassan, M. Kamel, S. Tong, R. Zane, Life-
586 Extended Active Battery Control for Energy Storage Using Electric Ve-
587 hicle Retired Batteries, IEEE Trans. Power Electron. 38 (6) (2023) 6801–
588 6805. doi:10.1109/TPEL.2023.3252362.